



Effects of Wavy Channel Entrance Design on Streamwise Counter-rotating Vortices: a Visualization Study

A. C. Budiman^{1†}, H. Mitsudharmadi², Y. Bouremel³, S. H. Winoto⁴ and H. T. Low¹

¹Department of Mechanical Engineering, National University of Singapore, 9 Engineering Drive 1, Singapore 117576

²Reactive Flow Modeling Laboratory Group in Clean Combustion Research Center, King Abdullah University of Science and Technology, Thuwal 23955, Kingdom of Saudi Arabia

³Institute of Ophthalmology, University College London, London EC1V 9EL, United Kingdom

⁴Faculty of Engineering, Universitas Diponegoro, Tembalang Campus, Semarang 50275, Indonesia

†Corresponding Author Email: christantho@u.nus.edu

(Received September 30, 2015; accepted December 11, 2015)

ABSTRACT

Two different channel entrance designs, code named Valley First (VF) and Peak First (PF), were experimentally visualized by means of smoke-wire visualization technique to observe their effects towards the streamwise counter-rotating vortices generated. The spanwise wavelength of the vortices was pre-set by modifying the leading edge. The investigation was carried out on the laminar boundary-layer flow in a rectangular channel with one-sided wavy surface that has amplitude a and wavelength λ of 7.5 mm and 76 mm, respectively. The vortices in the channel with VF design preserve farther downstream than those on the PF design, which might be caused by the large favorable pressure gradient between the entrance flat plate and the first peak location. The counter-rotating vortices could still be observed at non-dimensionalized streamwise distance χ ($= x/\lambda$) = 2.47 for Reynolds number Re ($= UH/\nu$) = 9900 in channel with VF design. For lower Re , the vortices could preserve further downstream. In contrast, in channel with PF design, the structures were only visible clearly up to approximately $\chi = 1.32$ for $Re = 4700$ and $\chi = 0.39$ for $Re = 5200$.

Keywords: Boundary-layer flow; Smoke-wire flow visualization; Wavy channel.

NOMENCLATURE

a	amplitude of wavy surface	x, y, z	Cartesian coordinates system for streamwise, normal, and spanwise direction, respectively
H	channel height (in y -direction)		
Re	Reynolds number		
U	streamwise fluid velocity		
U_D	streamwise fluid velocity at downwash	λ	wavelength of wavy surface
U_U	streamwise fluid velocity at upwash	ν	fluid kinematic viscosity
		χ	non-dimensional streamwise distance

1. INTRODUCTION

Wavy surface in channel flow has been used in many industrial engineering applications due to its benefits such as heat transfer and mixing enhancement (Bergles and Webb 1985; Rush *et al.* 1999). Compared with straight channel, it has been reported that wavy surface could produce substantial heat transfer augmentation, for example, in the turbulent flow in tube with periodic wavy wall (Sparrow and Prata 1983). The study has also been extended to the creep and laminar flow to achieve similar mass or heat transfer enhancement in other applications, for example in the membrane

blood oxygenators, electronic chip cooling system, or compact heat exchangers with fin-plate configurations (Nishimura *et al.* 1986; Patera and Mikic 1986).

One of the possible causes lies on the streamwise counter-rotating vortices, which can appear naturally or being induced by means of artificial roughness, perturbation wires (Peerhossaini and Bahri 1998) or modifications on the leading edge of the channel (Nishikawa *et al.* 2007). The natural streamwise counter-rotating vortices seem to occur due to the centrifugal imbalance caused by the curvature of the wavy surface, that is, when the centrifugal force overcomes the radial pressure

gradient (Aider *et al.* 2008).

The occurrence of the streamwise counter-rotating vortices causes a three-dimensional variation of boundary-layer thickness, which are similar to the so-called Görtler vortices on concave surface laminar boundary layer flow (Görtler 1940) and affect the flow transition to turbulence (Tani and Aihara 1969; Wortmann 1969). Chen *et al.* (1985) and Beckwith *et al.* (1985) also reported such transition cases in a supersonic nozzle in a laminar boundary-layer. An extensive review of such vortices and the mechanism with regards to flow transition is reported by Saric (1994).

The streamwise counter-rotating vortices travel downstream (x-direction in Cartesian coordinates) in form of horseshoe vortices and might transform into mushroom-like structure before breaking down due to the onset of turbulence. The presence of such vortices could result in mixing augmentation (Winoto *et al.* 2005) or, in contrast, loss of cooling efficiency in the hot rotating blades (Aider *et al.* 2008). The downstream development of this mushroom-like structure is strongly caused by the nonlinearities in the cross-sectional y-z plane, that is, the occurrence of the varicose mode instability as a secondary instability (Lee and Liu 1992). The mushroom-like structure itself consist of two finite regions namely the mushroom stem and hat. The mushroom stem coincides with the “upwash” region, that is, where the fluid is ejected from the surface resulting in a thicker boundary layer and lower shear stress. The fluid will return towards the wall in form of the mushroom hat. The region of maximum shear and thinnest boundary layer in between of two mushroom stems is called “downwash” region. The sketch of these two regions is shown in Fig. 1.

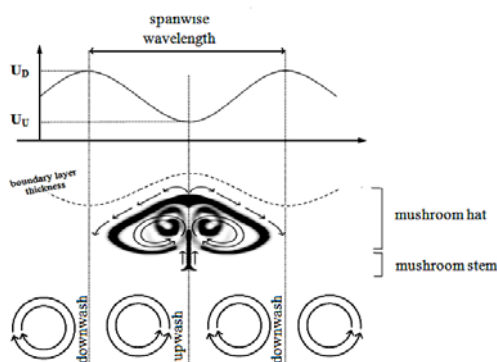


Fig. 1. Spanwise variation of streamwise velocity within a system of counter-rotating vortices showing the definition of “upwash” and “downwash” regions.

In this study, the downstream evolutions of the induced streamwise counter-rotating vortices in laminar boundary-layer flow with two channel entrance designs were qualitatively examined by means of smoke-wire flow visualization. The sketches of these two channel designs, code named Valley First and Peak First, are presented in Fig. 2. The difference between these two designs lies in the

connection between the entrance flat plate and the wavy surface at its valley or its peak. The channel with Valley First configuration is exposed to concave surface prior to the convex segment, which allows the acceleration of fluid flow. Furthermore, it is suspected that the centrifugal force field at the peak would give positive disturbance growth rate resulting in destabilizing effect to the main flow (Floryan 2001). In contrast, the flow in channel with Peak First design will encounter stabilizing effect beforehand. It is believed that besides the Reynolds number, the geometrical shapes of the channel with wavy surface could noticeably contribute to the amplification or weakening of the vortex disturbances.

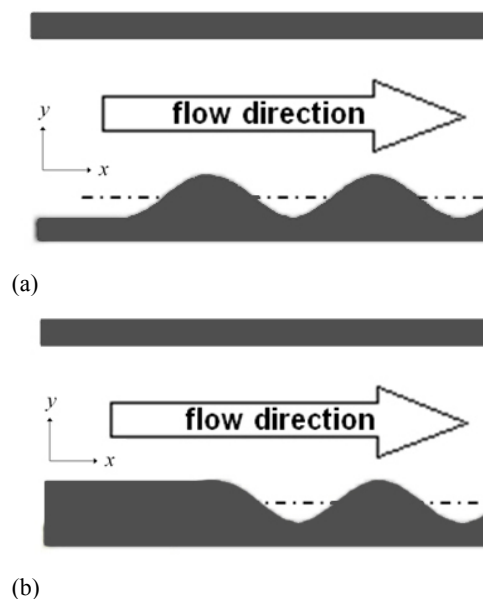


Fig. 2. Channel entrance designs: (a) Valley First (VF) and (b) Peak First (PF).

2. EXPERIMENTAL SET-UP

A 159 mm width rectangular cross-section acrylic channel with one-sided wavy surface is used in this experiment. The wavy surface is in the form of sinusoidal waves with amplitude a and wavelength λ of 7.5 mm and 76 mm, respectively. The length of the flat entrance plate prior to the wavy surface is 150 mm, almost twice the wavelength of the sinusoidal waves. Non-dimensional streamwise distance χ is defined as:

$$\chi = x/\lambda \tag{1}$$

where x is the streamwise distance measured from the leading edge. By applying this definition, the location of the first peak for the VF and PF entrance design is $\chi = 2.47$ and 1.97, respectively.

For better visualization conditions, the wavy surface of the channel was covered by a thin black matte film to reduce any reflections from the light source. The channel was mounted into the open-loop wind tunnel test section with a square cross-sectional area of 160 mm x 160 mm and contraction ratio of 9.8.

The free-stream turbulent intensity of the wind tunnel is less than 0.3% for velocity between 1 – 5 m/s.

Smoke-wire flow visualization technique was used in this study, similar to the previous study by Budiman *et al.* (2015). Paraffin oil is selected as smoke-generating fluid. A stainless steel wire of 0.193 mm diameter was installed upstream of the leading edge along the spanwise direction of the channel. The diameter of this wire is sufficiently thin in order to avoid the formation of von Karman vortex-street that would penetrate the boundary-layer. The wire was connected to a pressurized oil reservoir and pulled by a weight on the other end.

To generate a thin smoke layer, the wire was electrically heated by a DC power supply with a voltage ranging from 11 to 18 V and a current of 1000 to 1300 mA depending on the air velocity. A 50 mW green laser pointer (of wavelength = 532 nm) was used as a light source for this visualization. A transparent cylindrical rod is attached near the tip of the laser pointer to generate a laser sheet. A digital video camera was positioned perpendicular to the y-z plane far downstream of the wind tunnel to capture the visualization images without disturbing the air flow. The sketch of the wind tunnel and the smoke-wire flow visualization apparatus is presented in Fig. 3(a).

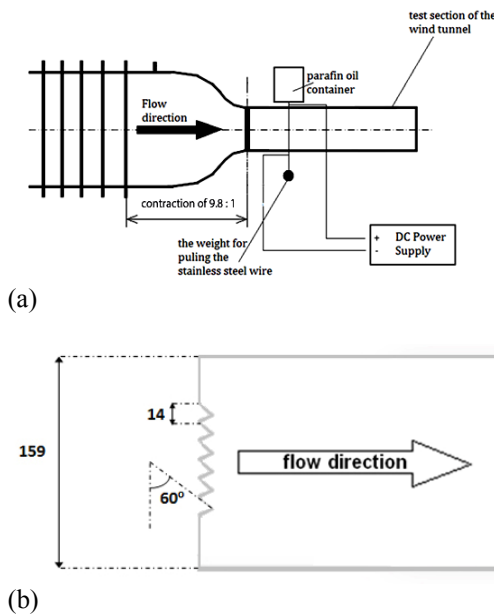


Fig. 3. Experimental setup: (a) the wind tunnel and the smoke-wire flow visualization setup and (b) the modification of the plate leading edge by means of zigzag pattern cut. The dimensions are in mm.

Since naturally developed streamwise counter-rotating vortices generally would have a variation in their spanwise wavelength and growth rate, unless great care is taken in the fabrication of the channel and in controlling the flow condition, it is necessary to pre-set the streamwise counter-rotating vortices.

To do this, a modification of the plate leading edge in the form of equilateral zigzag pattern is applied (Nishikawa *et al.* 2007). The spanwise base length is 14 mm, as depicted in Fig. 3(b). This method has been proven to successfully generate streamwise counter-rotating vortices with nearly uniform spanwise wavelength, which would be useful to avoid subjectivity and difficulty in studying the downstream evolution of the structures (Wortmann 1969; Winoto *et al.* 2005; Budiman *et al.* 2015).

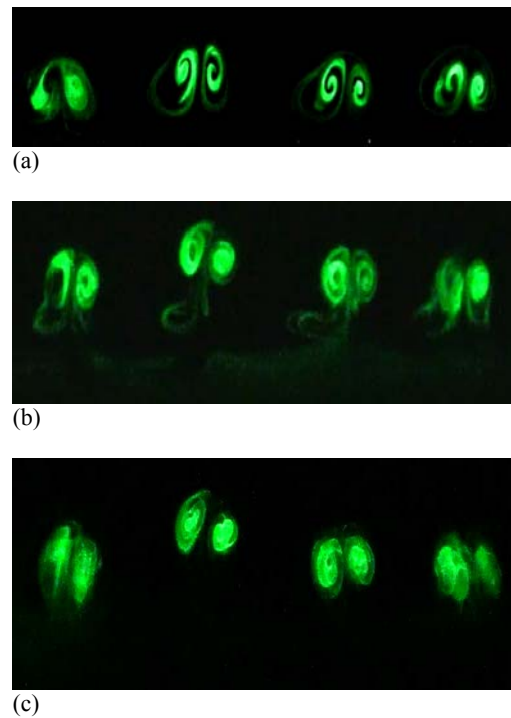


Fig. 4. Downstream development of streamwise counter-rotating vortices in the channel with the VF entrance design and $Re = 6800$ at various streamwise locations: (a) first peak ($\chi = 2.47$), (b) first valley ($\chi = 2.97$), and (c) second peak ($\chi = 3.47$).

3. RESULTS AND DISCUSSION

The appearance of streamwise counter-rotating vortices can be distinguished by a spanwise variation of boundary-layer thickness. Fig. 4 shows the visualization of streamwise counter-rotating vortices at Reynolds number $Re = UH/\nu = 6800$ for the VF entrance designs at various streamwise locations. The channel height H is the distance between two parallel flat plates at the leading edge. Mean velocity U is also measured at the leading edge. Four counter-rotating vortices with nearly the same spanwise wavelength were clearly observed at the first peak of the wavy surface ($\chi = 2.47$) in Fig. 4(a). The difference between each vortex structure was probably caused by the imperfections of the zigzag pattern cut or the wavy surface itself. According to the visualization images, this minor difference was still tolerable for this qualitative study. Due to the average size of the vortices which was smaller than 7.5 mm (the amplitude of the

wavy surface), the camera could not record the streamwise vortices at $\chi < 2.47$ for a channel with VF entrance design.

After the first peak, the vortices were floating above a separation bubble formed in the valley that appears in dark green at the bottom of Fig. 4(b). This formation of separation bubble is in conjunction with the study by Loh and Blackburn (2011). The structure was still noticeable at the second peak ($\chi = 3.47$) before it became more indistinct as it travels further downstream prior to its breakdown.

The effects of Reynolds number on the structure of the vortices in a channel with VF design is depicted in Fig. 5. The counter-rotating structure remained visible at the first peak of the wavy surface up to $Re = 9900$, where more engulfment occurred and this can be attributed to the mixing enhancement (Baldyga and Bourne 1984). At higher Reynolds number, the structure became more indistinct. This might indicate the condition where the mushroom-like structure was almost breakdown prior to turbulence.

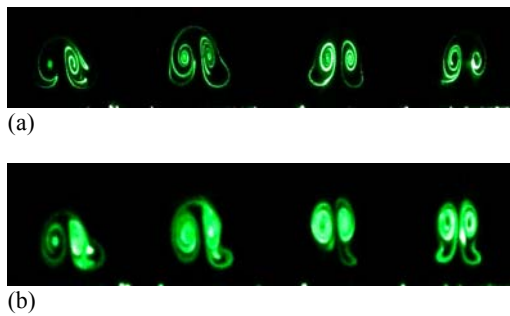


Fig. 5. Downstream development of streamwise counter-rotating vortices in the channel with the VF entrance design at the first peak ($\chi = 2.47$) for: (a) $Re = 7800$ and (b) $Re = 9900$.

When amplitude of the wavy surface is doubled from the amplitude used in the earlier study by Budiman *et al.* (2015), it is found that the streamwise counter-rotating vortices have a notably different appearance, regardless of the Reynolds number. Budiman *et al.* (2015) presented streamwise counter-rotating vortices with a relatively long mushroom stem and small mushroom hat. In contrast, due to larger amplitude used in this study, the mushroom hat was much bigger, as depicted in Figs. 4 and 5. The stronger curvature of the wavy surface means less energy for the upwash movement of the vortices to penetrate the mean flow before moving back towards the wavy surface. As a result, the mushroom stem was much shorter even as the amplitude of the wavy surface increases, despite keeping the same ratio of amplitude over channel height.

The presence of large favorable pressure gradients from the protuberance in a channel with VF entrance design is suspected to delay the breakdown of the counter-rotating vortices. Patel

and Head (1968), and subsequently, Finnicum and Hanratty (1988) discussed the possibility of reverse transition from turbulent boundary layer flow to be in the laminar state when encountering rapid increase of mean velocity. In addition to the induced disturbance, the centrifugal imbalance from the concave surface might contribute to stronger upwash, making the vortex structure less vulnerable to breakdown. As such, it is understandable when the vortices diffused much earlier on a channel with PF entrance (which is exposed to adverse pressure gradient at $\chi = 1.97$ that decreases the fluid velocity), as shown in Figs. 6 and 7. In Fig. 6, the vortices were completely disappeared although it was still at the entrance flat plate, that is, at $\chi = 1.32$, less than half the distance downstream recorded in the VF design. It is worth mentioning that the Reynolds number was only 5200, more than 20 per cent lower compared with the previous visualization with the VF entrance design (Fig. 4).

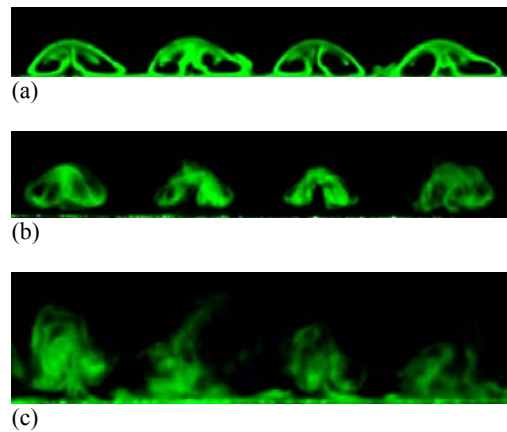


Fig. 6. Downstream development of streamwise counter-rotating vortices in the channel with the PF entrance design and $Re = 5200$ at various streamwise location: (a) $\chi = 0.13$, (b) $\chi = 0.39$, and (c) $\chi = 1.32$.

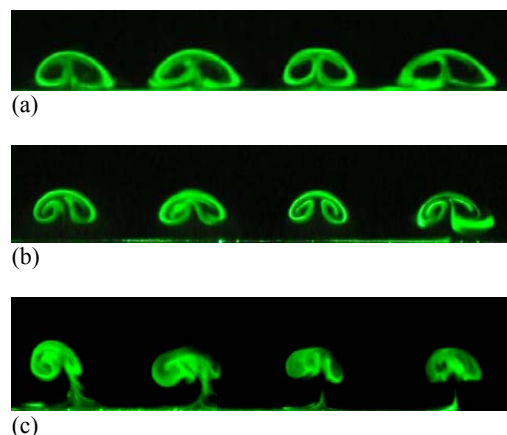


Fig. 7. Downstream development of streamwise counter-rotating vortices in the channel with the PF entrance design and $Re = 4700$ at various streamwise location: (a) $\chi = 0.13$, (b) $\chi = 0.39$, and (c) $\chi = 1.32$.

Figure 6 shows the evolution of the vortices induced by the leading edge modifications (Fig. 6(a)) into mushroom-like structures (Fig. 6(b)) in a channel with the PF entrance design. As shown in Fig. 6(c), at this streamwise distance ($\chi = 1.32$), the mushroom hats were no longer visible, while four mushroom stems were still slightly distinguishable near the bottom surface.

Figure 7 shows the streamwise counter-rotating vortices at $Re = 4700$ in the channel with the PF entrance design, which has slightly longer mushroom stems compared to Fig. 6 and could travel farther downstream before breakdown. As depicted in Fig. 7(c), the mushroom-like structures were still clearly visible at $\chi = 1.32$. However the structures were already blurred before reaching the similar streamwise distance as in the channel with VF entrance design. From these comparisons, it can be concluded that the use of VF entrance design in the channel could delay the breakdown of the counter-rotating vortices into turbulence further downstream than the PF entrance design.

4. CONCLUSION

Smoke-wire flow visualization method has been used to observe the streamwise development of counter-rotating vortices in a laminar boundary-layer flow on a rectangular channel with a wavy surface. Two channel entrance designs were investigated, based on the connection between the flat entrance plate and the wavy surface. From the visualization, it is found that the vortices remain visible at non-dimensionalized streamwise distance $\chi = 2.47$ for Reynolds numbers close to ten thousand in a channel with the Valley First (VF) entrance design. In contrast, the structure was already diffused for comparable streamwise locations and at lower Reynolds number for the Peak First (PF) design, on which there were no large favorable pressure gradient at the end of the entrance flat plate. Based on these results, a channel with the VF design is able to maintain the appearance of the vortices on a longer streamwise distance than the channel with the PF entrance design.

REFERENCES

- Aider, J. L., Duriez, T. and J. E. Wesfreid (2008). From natural to forced counter-rotating streamwise vortices in boundary layers. *Journal of Physics: Conference Series* 137, 012009.
- Baldyga, J. and J. R. Bourne (1984). A fluid mechanical approach to turbulent mixing and chemical reaction part II micromixing in the light of turbulence theory. *Chemical Engineering Communications* 28, 243-258.
- Beckwith, I. E., M. R. Malik, F. J. Chen and D. M. Bushnell (1985). Effects of nozzle design parameters on the extent of quiet test flow at Mach 3.5, *Laminar-Turbulent Transition*, pp. 589-600. Springer-Verlag, New York, USA.
- Bergles, E. A. and R. L. Webb (1985). A guide to the literature on convective heat transfer augmentation. *the 23rd National Heat Transfer Conference*. Denver, USA.
- Budiman, A. C., H. Mitsudharmadi, Y. Bouremel, S. H. Winoto and H. T. Low (2015). Visualization of pre-set vortices in boundary layer flow over wavy surface in rectangular channel. *Journal of Visualization* 18, 669-677.
- Chen, F. J., M. R. Malik and I. E. Beckwith (1985). Instabilities and transition in the wall boundary layers of low-disturbance supersonic nozzles. *AIAA 18th Fluid Dynamics and Plasmadynamics and Lasers Conference*. Cincinnati Ohio, USA. AIAA-85-1573.
- Finnicum, D. S. and T. J. Hanratty (1988). Effect of favorable pressure gradients on turbulent boundary layers. *AIChE Journal* 34(4), 529-540.
- Floryan, J. M. (2001). Centrifugal instability of Couette flow over a wavy wall. *Physics of Fluids* 14(1), 312-322.
- Görtler, H. (1940). Über eine dreidimensionale Instabilität laminarer Grenzschichten an konkaven Wänden. *Ges. D. Wiss. Göttingen. Nachr. a. d. Math* Vol. 2; translated in 1954 as On the three-dimensional instability of laminar boundary layers on concave walls. *NACA TM* 1375, 1-32.
- Lee, K. and J. T. C. Liu (1992). On the Growth of mushroomlike structures in nonlinear spatially developing Görtler vortex flow. *Physics of Fluids A* 4, 95-103.
- Loh, S. A. and H. M. Blackburn (2011). Stability of steady flow through an axially corrugated pipe. *Physics of Fluids* 23, 111703
- Nishikawa, H., K. Akaishi and A. Ito (2007). Visualization of secondary instability flows generated between Görtler vortices (continued paper). *Journal of Visualization Society of Japan* 27, 25-26.
- Nishimura, T., Y. Kajimoto and Y. Kawamura (1986). Mass transfer enhancement in channels with a wavy wall. *Journal of Chemical Engineering of Japan* 19(2), 142-144.
- Patel, V. C. and M. R. Head (1968). Reversion of turbulent to laminar flow. *Journal of Fluid Mechanics* 34(02), 371-392.
- Patera, A. T. and B. B. Mikic (1986). Exploiting hydrodynamic instabilities. Resonant heat transfer enhancement. *International Journal of Heat and Mass Transfer* 29(8), 1127-1138.
- Peerhossaini, H. and F. Bahri (1998) On the spectral distribution of the modes in nonlinear Görtler instability. *Experimental Thermal and Fluid Science* 16, 195-208.
- Rush, T. A., T. A. Newell and A. M. Jacobi (1999). An experimental study of flow and heat transfer in sinusoidal wavy passages.

- International Journal of Heat and Mass Transfer* 42, 1541-1553.
- Saric, W. S. (1994). Görtler vortices. *Annual Review of Fluid Mechanics* 26, 379-409.
- Sparrow, E. M. and A. T. Prata (1983). Numerical solutions for laminar flow and heat transfer in a periodically converging-diverging tube, with experimental confirmation. *Numerical Heat Transfer* 6, 441-461.
- Tani, I. and Y. Aihara (1969). Görtler vortices and boundary-layer transition. *Zeitschrift für angewandte Mathematik und Physik* 20(5), 609-618.
- Winoto, S. H., H. Mitsudharmadi and D. A. Shah (2005). Visualizing Görtler vortices. *Journal of Visualization* 8(4), 315-322.
- Wortmann, F. X. (1969). Visualization of Transition. *Journal of Fluid Mechanics* 38(3), 473-480.